# Bulletin of the Seismological Society of America

## On the Rupture Process of the August 23, 2011, Virginia Earthquake

--Manuscript Draft--

| | |
|---|---|
| **Manuscript Number:** | BSSA-D-12-00229 |
| **Article Type:** | Article |
| **Section/Category:** | Regular Issue |
| **Full Title:** | On the Rupture Process of the August 23, 2011, Virginia Earthquake |
| **Corresponding Author:** | Martin C. Chapman<br>Virginia Polytechnic & State University<br>Blacksburg, VA UNITED STATES |
| **Corresponding Author's Institution:** | Virginia Polytechnic & State University |
| **Corresponding Author E-Mail:** | mcc@vt.edu |
| **Order of Authors:** | Martin C. Chapman |
| **Abstract:** | The M 5.7, August 23, 2011 Virginia earthquake was studied using local and teleseismic recordings. The earthquake was a shallow reverse rupture in the central Virginia seismic zone. The epicenter was at 37.905°N, 77.975°W, with focal depth 8.0 km. A few local stations recorded both the mainshock and several of the larger aftershocks. This allowed location of the mainshock epicenter relative to the accurate locations of aftershocks recorded by a temporary deployment of stations. The aftershocks define a tabular zone oriented in near-perfect agreement with the mainshock focal mechanism nodal plane. The mainshock focal depth was determined by comparing teleseismic waveforms with synthetics. Local and teleseismic recordings show a complex rupture. The diverse data set was used to locate two large subevents relative to a small initial subevent. The initial slip episode had moment of roughly 2.5 x 1016 N•m, and was followed 0.75 seconds later by a subevent with a moment of approximately 2.3 x1017 N•m that amounted to approximately 60% of the total moment release. A third subevent with moment 1.2 x1017 N•m occurred 1.57 seconds after rupture initiation. Rupture initiated near the southwestern corner of the aftershock zone and proceeded to the northeast along strike and up-dip. The mainshock rupture occurred at the base of the early aftershock zone. The three subevents involved a compact fault area: the estimated distance between the initial and final subevent is only 2.0 km. However, the total rise time of the earthquake is large in comparison to the fault rupture area and the origin time difference between subevents indicates a slow rupture velocity of 1.3 to 1.7 km/s. This was a consequence of the rupture being comprised of two short-duration energetic slip-events that were well-separated in time along with a small, possibly low stress-drop, initiation event. |
| **Author Comments:** | |
| **Suggested Reviewers:** | |
| **Opposed Reviewers:** | |

*Powered by Editorial Manager® and Preprint Manager® from Aries Systems Corporation*

Letter to Editor
Click here to download Letter to Editor: covertlet.doc

Virginia Tech
VIRGINIA POLYTECHNIC INSTITUTE
AND STATE UNIVERSITY

**Seismological Observatory**

Department of Geosciences
4044 Derring Hall, Blacksburg, Virginia 24061-0420
Telephone: (540) 231-5036 Fax: (540) 231-3386
E-mail: mcc@vt.edu
Homepage: http://www.geol.vt.edu/profs/mcc/

Dear BSSA Editor:

I am submitting for possible publication in the BSSA a paper entitled "On the Rupture Process of the August 23, 2011, Virginia Earthquake."

Dr. Martin Chapman

Martin Chapman

Research Associate Professor

Manuscript
Click here to download Manuscript: chapman_bssa_submit.docx

# On the Rupture Process of the August 23, 2011 Virginia Earthquake

**M.C. Chapman**

**Department of Geosciences**

**Virginia Tech**

**4044 Derring Hall**

**Blacksburg, VA 24061**

**mcc@vt.edu**

**ph: (540) 231-5036**

**Submitted to**

**Bulletin of the Seismological Society of America**

**July 5, 2012**

## Abstract

The M 5.7, August 23, 2011 Virginia earthquake was studied using local and teleseismic recordings. The earthquake was a shallow reverse rupture in the central Virginia seismic zone. The epicenter was at 37.905°N, 77.975°W, with focal depth 8.0 km. A few local stations recorded both the mainshock and several of the larger aftershocks. This allowed location of the mainshock epicenter relative to the accurate locations of aftershocks recorded by a temporary deployment of stations. The aftershocks define a tabular zone oriented in near-perfect agreement with the mainshock focal mechanism nodal plane. The mainshock focal depth was determined by comparing teleseismic waveforms with synthetics. Local and teleseismic recordings show a complex rupture. The diverse data set was used to locate two large subevents relative to a small initial subevent. The initial slip episode had moment of roughly $2.5 \times 10^{16}$ N·m, and was followed 0.75 seconds later by a subevent with a moment of approximately $2.3 \times 10^{17}$ N·m that amounted to approximately 60% of the total moment release. A third subevent with moment $1.2 \times 10^{17}$ N·m occurred 1.57 seconds after rupture initiation. Rupture initiated near the southwestern corner of the aftershock zone and proceeded to the northeast along strike and up-dip. The mainshock rupture occurred at the base of the early aftershock zone. The three subevents involved a compact fault area: the estimated distance between the initial and final subevent is only 2.0 km. However, the total rise time of the earthquake is large in comparison to the fault rupture area and the origin time difference between subevents indicates a slow rupture velocity of 1.3 to 1.7 km/s. This was a consequence of the rupture being comprised of two short-duration energetic slip-events that were well-separated in time along with a small, possibly low stress-drop, initiation event.

## Introduction

The M 5.7, August 23, 2011 earthquake in central Virginia was felt over most of the eastern seaboard of the United States. It caused MM VIII damage near the epicenter in Louisa County, Virginia, and minor damage over a region that included Washington, DC.

Taber (1913) noted a long history of seismicity in central Virginia. Bollinger (1969, 1973a, 1973b) recognized a central Virginia seismic zone, that includes several central Virginia counties, and includes that part of the Virginia Piedmont geologic province within approximately 60 km of the James River, between Charlottesville, on the west and Richmond, on the east. Prior to 2011, the largest shock in the seismic zone was the December 22, 1875 event, of magnitude approximately 4.5 - 5.0. Recently, on December 9, 2003, a compound M 4.5 earthquake occurred approximately 20 km to the southwest of the 2011 earthquake and was felt widely throughout the middle Atlantic region (Kim and Chapman, 2005).

Seismic network monitoring in central Virginia began in the 1970's. The focal mechanisms show a wide range of nodal plane orientation, with both reverse and strike-slip mechanisms (Munsey and Bollinger, 1985; Bollinger et al., 1991; Kim and Chapman, 2005). The focal mechanism P axes tend to be sub-horizontal, but range in azimuth from northeast to southeast. Focal depths are in the range from near-surface to approximately 12 km, with the median depth at 8 km. The geologic structure of the upper crust is complex. The major structural fabric is the result of low-angle thin-skinned thrusting during the late Paleozoic, but high-angle faults exist throughout the area as the result of extension in the early Mesozoic. The earthquakes occur within allochthonous crystalline rocks of Paleozoic age, above the basal Appalachian detachment inferred at a depth of approximately 12 km from seismic reflection profiles in the area (Coruh et al., 1988; Pratt et al., 1988, Bollinger et al., 1991). Although there are several Mesozoic extensional basins in the central Virginia area (Culpeper, Farmville, Scottsville, and Richmond basins), the seismicity is not clearly associated with mapped Mesozoic faults.

As was the case with the 2003 compound earthquake, the 2011 mainshock was recorded by only a few stations at local distances, and the initial mainshock location was uncertain to such an extent that no meaningful geological inferences could be drawn from it. A triggered strong motion recording at the Dominion, Inc., North Anna power station, approximately 23 km to the northeast of the actual epicenter represents the best local recording of this event. Other stations at local to near-regional distance that recorded the mainshock, with variable quality, are shown in Figure 1. In contrast to the situation with the main shock, teams from universities, IRIS and the US Geological Survey converged on the epicentral area in the days following the mainshock and the prolific aftershock sequence was well-recorded.

This study examines the rupture process of the mainshock. Both local and teleseismic data show evidence of a complex rupture, consisting of a weak initiation pulse followed by two larger subevents, all clearly separated in time. The early aftershock hypocenters define a tabular zone oriented in near-perfect agreement with the mainshock focal mechanism. The objective of the study was to locate the subevents comprising the mainshock in time and space. The analysis was not straight-forward because of the sparse near-source data. It involved several assumptions, and relies heavily on teleseismic recordings. As described in more detail below, a velocity model for the upper crust was derived from aftershock arrival time data. I assumed that the subevents comprising the mainshock occurred on a single fault plane, with strike and dip defined by the mainshock focal mechanism and the geometry of the early aftershock hypocenters. On the basis of that assumption, I located the two large subevents relative to the initial small subevent, using teleseismic and local data. Finally, the focal depth of the mainshock was determined from the teleseismic data, and the epicenter was located relative to the accurately determined epicenters of the largest aftershocks using data recorded by the temporary station deployment as well as by the few permanent local stations that had also recorded the mainshock.

### Aftershocks

Figure 2 shows the locations of temporary stations deployed nearest the mainshock epicenter as well as the epicenter locations of larger aftershocks that occurred prior to January 12, 2012. I focused on the early aftershocks that occurred from August 26 through September 2, 2011. The best-recorded subset of those events is plotted in perspective in Figure 3. A plane was fit by least-squares to the hypocenters forming the western cluster of events in Figure 3, with the result being an inferred fault plane strike of N29°E and dip of 51 degrees to the southeast. The USGS/St. Louis University moment tensor solution is: strike N28°E, dip 50°, rake 113°, focal depth 6 km, moment magnitude Mw 5.65 (Herrmann, 2011). The aftershocks are notable for their shallow depth (most are shallower than 6 km) and the fact that some of the earliest aftershocks occurred in a compact cluster that is approximately 10 km to the northeast of the larger cluster of aftershock hypocenters than appear to define the mainshock fault plane.

### Velocity Model

The velocity model routinely used for hypocenter location in central Virginia by the Virginia Tech Seismological Observatory (VTSO) since 1978 was derived from an 80 km, reversed refraction profile that used quarry blasts for sources (Bollinger et al., 1980). The model features a two layer crust. The upper layer is 15 km thick with *P* and *S*-velocities of 6.09 and 3.53 km/s, respectively. The lower crust is represented by a layer 21 km thick with *P* and *S*-

velocities 6.50 and 3.79 km/s, respectively. The $P_n$ and $S_n$ velocities are 8.18 and 4.73 km/s, respectively. The Moho dips to the west beneath the central Virginia seismic zone: beneath the Blue Ridge Mountains to the west of Charlottesville, Virginia crustal thickness is approximately 39 km, and approximately 31 km beneath Richmond.

This study required an accurate estimate of the *P* and *S*-wave velocities for the shallow crust containing the mainshock and the aftershocks. Thirty-six of the best-recorded aftershocks were selected for analysis. Because of the small source-station distances, a half-space velocity model was assumed. The *S*-*P* arrival time intervals at the temporary stations recording those aftershocks were used to estimate the origin times and *P/S* velocity ratio, using a joint inversion based on the well-known Wadati method. The hypocenters were then estimated using the location program HYPOELLIPSE (Lahr, 1999) with the origin times fixed and an initial trial estimate of the *P*-wave velocity. The resulting epicenter distances and the observed travel times were then used to obtain an updated joint estimate of the *P*-wave velocity. The HYPOELLIPSE location was repeated and a new estimate of the *P*-wave velocity was obtained. This iterative process was repeated, until the velocity estimate was unchanged from previous iterations. In detail, let

$$T_s - T_p = \left(O + {}^{x}/_{v_s}\right) - \left(O + {}^{x}/_{v_p}\right) = x\left({}^{1}/_{v_s} - {}^{1}/_{v_p}\right), \qquad (1)$$

where *Ts*-*Tp* is the difference between *P*-wave and *S*-wave arrival times, *O* is the earthquake origin time, $v_p$ is the *P*-wave velocity and

$$x = \left(T_p - O\right)v_p. \qquad (2)$$

Substitution of Equation 2 for *x* into Equation 1 gives

$$T_s - T_p = -O\left({}^{v_p}/_{v_s} - 1\right) + \left({}^{v_p}/_{v_s} - 1\right)T_p \ . \tag{3}$$

A linear plot of the *S-P* arrival time interval versus the *P*-wave arrival time (Wadati Plot) allows one to estimate the velocity ratio from the slope and the earthquake origin time from the intercept of Equation 3.

Assuming a half-space velocity structure, and data from i = 1,2,...n different earthquakes recorded by a network of j = 1,2,....m stations, we have a system of observational equations of the form

$$\left[T_s - T_p\right]_{ij} = -O_i\left({}^{v_p}/_{v_s} - 1\right) + \left({}^{v_p}/_{v_s} - 1\right)\left[T_p\right]_{ij}. \tag{4}$$

This system was solved by the method of least-squares to estimate the origin time of the i'th earthquake and the velocity ratio. For the same half-space velocity structure, and given an initial estimate of the epicenter, along with the origin time estimates, I proceeded to determine estimates of the *P*-wave velocity and focal depths from the linear relationship between the *P*-wave travel time squared and the epicentral distance squared. For several earthquakes recorded by a network of stations, we have

$$\left(\left[T_p\right]_{ij} - O_i\right)^2 = \ [h_i]^2\ \left({}^{1}/_{v_p}\right)^2 + \left({}^{1}/_{v_p}\right)^2\left[x_{ij}\right]^2 , \tag{5}$$

a system of equations that can be solved using the method of least squares to determine $v_p$ and the focal depth *h* of the i'th earthquake. Figure 4a shows the data and joint estimate of the slope of Equation 4. Figure 4b shows the residuals plotted versus epicenter distance (squared) for Equation 5. The estimate of $v_p/v_s$ is 1.69 +/- 0.01 and $v_p$ is 5.96 +/- 0.06 km/s.

**Evidence of Source Complexity**

Figure 5 plots the acceleration and velocity recordings from a strong-motion instrument at foundation level in the Unit 1 containment structure at the Dominion, Inc., North Anna power station, 23 km from the epicenter, along a source-receiver azimuth of N54°E. The instrument triggered during the *P*-wave portion of the signal. The transverse component motion shows three *S*-wave pulses, indicated in Figure 5a, at 1.2, 1.7 and 2.5 seconds after the trigger-time. Figure 5b shows the recorded transverse motion in comparison with a full-wavefield synthetic generated from a finite-fault simulation of an M 6.0 shock, focal depth 7.5 km, 10 MPa static stress drop, for a receiver at the corresponding source-receiver distance and azimuth. The focal mechanism used for the synthetic differs only slightly from that of the earthquake: the synthetic assumes a hypocentral depth of 7.5 km,: pure reverse motion (rake angle 90 degrees, compared to 113 degrees for the earthquake) and fault dip of 45 degrees compared to 51 degrees for the actual earthquake. The synthetic motions and the simulation method are described in detail by Chapman and Godbee (2012). The point of this comparison is the fact that the real data show a second large *S*-wave pulse following the far-field *S*-wave arrival of the synthetic, as well as a possible earlier precursor. The identical polarities of the three observed *S*-wave pulses are consistent with that of the synthetic far-field *S*-wave arrival, suggesting that these are source effects, and are not due to multi-pathing.

Teleseismic *P*-wave arrivals at several stations exhibit pulses consistent with those recorded at North Anna. Figure 7 shows velocity recordings at some of those stations. Figure 8 indicates the locations of 17 teleseismic stations where the subevent arrivals could be discriminated from the *pP* an *sP* surface reflections with the aid of waveform simulations and arrival times could be accurately determined.

**Teleseismic Waveform Simulation**

The shallow focal depth of the earthquake complicates interpretation of the teleseismic signals in terms of possible subevent arrivals. Simple synthetic seismograms containing the *P*, *pP* and *sP* phases were constructed to aid in identification of the subevent signatures at the various receivers. A half-space Earth model was assumed. The fault strike, dip and rake assumed for the simulations are N29°E, 51°, 113°, respectively. A constant ray parameter was assumed for the three phases, taken from the tables of observed times of *P*, surface focus (Herrin and Seismological Society of America, 1968). The vertical component of ground displacement was simulated as follows:

$$U(\omega) = CS(\omega)A(\omega)\left[R^{p} + R^{sP}F_{sp}\exp(i\omega T_{sP-P}) + R^{pP}F_{pp}\exp\,(i\omega T_{pP-P})\right]. \qquad (6)$$

In Equation 6, C is a constant representing net frequency-independent amplitude change due to impedance contrasts along the path, geometrical spreading and the free surface effect at the receiver, $S(\omega)$ is the source moment-rate, $A(\omega)$ is a causal attenuation operator, $R^P$, $R^{sP}$ and $R^{pP}$ are the radiation pattern values for the direct *P*, *sP* and *pP* phases, that depend on ray take-off angles  and source-receiver azimuth ( Aki and Richards, 2002, Equations 4.89 and 4.90), and $F_{pp}$ and $F_{sp}$ are the coefficients for *P-to-P* and *S-to-P* reflection at the free surface (Aki and Richards, 2002, Equations 5.27 and 5.31).

The time intervals between *P* and the surface reflections *pP* and *sP* are represented in Equation 6 by $T_{pP-P}$ and $T_{sP-P}$, respectively. Assuming that ray parameter *p* is the same for the three phases, and referring to Figure 8, we have

$$T_{pP-P} = 2ph\,\cot(\mathrm{i}) = \frac{2h\cos(i)}{\alpha}, \tag{7}$$

$$T_{sP-P} = ph[\cot(j) + \cot(\mathrm{i})] = h\left[\frac{\cos(j)}{\beta} + \frac{\cos(i)}{\alpha}\right], \tag{8}$$

$$p = \frac{\sin(i)}{\alpha} = \frac{\sin(j)}{\beta}, \tag{9}$$

where α and β are *P*-wave and *S*-wave velocities, respectively.

The source moment-rate used for the simulation, *S(ω)* in Equation 6, is based on the Brune (1970) model and is given by

$$S(\omega) = \frac{M_o}{\left[1 - \frac{i\omega}{\omega_c}\right]^2}\ , \tag{10}$$

where the corner frequency $\omega_c$ is given by

$$\omega_c = 308.2\,\beta\,\left(\frac{\Delta\sigma}{M_o}\right)^{1/3}, \tag{11}$$

for β in m/s, stress drop Δσ in MPa and static moment $M_o$ in N·m.

The complex rupture comprised of n subevents was modeled by summing time-shifted displacements $U_i(\omega)$, i = 1,2,....n according to

$$U_c(\omega) = CA(\omega)\ \sum_{i=1}^{n} U_i(\omega) exp(i\omega\tau_i)\ . \tag{12}$$

The quantity $\tau_i$ in Equation 12 represents the time of the subevents and each $U_i$ is evaluated using Equation 6 with *C* = 1, and *A(ω)* =1, and with appropriate values for *h*, $M_o$ and $\Delta\sigma$ for the ith subevent. The ray parameter *p* is constant in the summation. The attenuation operator *A(ω)* and the amplitude normalization factor $C$ are applied to the summation of subevent displacements in Equation 12. The attenuation operator used here is represented by

$$A(\omega) = exp\left[-\frac{\omega t^*}{2} + iH(-\omega t^*/2)\right]. \tag{13}$$

In Equation 13, $H$ is the Hilbert transform. The phase of $A(\omega)$ is the Hilbert transform of the natural logarithm of the amplitude spectrum, and $A(\omega)$ is causal and minimum phase. The quantity $t^*$ as a function of distance for $P$-waves in the mantle was taken from Hwang and Ritsema (2011):

$$t^* = 0.592 + 0.0036\Delta \ \ for\ \Delta \geq 30\ degrees, \tag{14}$$

$$t^* = 0.7 \qquad for\ \Delta < 30\ degrees. \tag{15}$$

**Determination of Subevent Relative Locations**

Consider two sources, at points $O$ and $P$ in the fault plane (Figure 9). Define point $O$ to be the origin of a 3-dimensional Cartesian coordinate system, with the $X$-$Y$ plane horizontal, positive $Z$ axis upward and positive $X$ axis in the fault strike-direction. Let $\boldsymbol{V}_{op}$ be the position vector of point $P$, and let $\boldsymbol{V}_r$ be a unit vector in the direction of the $P$-wave ray to a receiver at infinity (the same ray parameter at O and P). Assume a constant near-source $P$-wave velocity $\alpha$. From Figure 9 we have the following expressions for the vectors $\boldsymbol{V}_{op}$ and $\boldsymbol{V}_r$.

$$\boldsymbol{V}_{op} = [I\vec{x}, Jcos(d)\vec{y}, Jsin(d)\vec{z}], \tag{16}$$

$$\boldsymbol{V}_r = [sin(toa)\cos(s-a)\,\vec{x}\,, \sin(toa)\sin(s-a)\vec{y}, -\cos(toa)\vec{z}], \tag{17}$$

where $s$ is strike of the fault, $d$ is the dip of the fault, $a$ is source-to-receiver azimuth and $toa$ is the ray take-off angle, given by

$$toa = sin^{-1}(p\alpha). \tag{18}$$

The *P*-wave arrival time difference $t_{p\text{-}o}$ for a receiver at infinity is given by

$$t_{p-o} = [\tau_p - \tau_o] - (V_{op} \cdot V_r)/\alpha \ , \tag{19}$$

where $V_{op} \cdot V_r$ is the scalar projection of $\boldsymbol{V}_{op}$ in the direction of $\boldsymbol{V}_r$ and $\tau_p$ and $\tau_o$ are the origin times at P and O, respectively. Using Equations 16 and 17, Equation 19 can be written as

$$t_{p-o} = [\tau_p - \tau_o] - \frac{Isin(toa)\cos(s-a)}{\alpha} + \frac{J[\sin(d)\cos(toa) - \cos(d)\sin(toa)\sin(s-a)]}{\alpha}. \tag{20}$$

The unknowns in Equation 20 are *I*, *J* and the origin time difference $\tau_p$ - $\tau_o$. The quantities *I* and *J* define the position of point *P* in a two-dimensional Cartesian coordinate system lying in the fault plane with origin at *O*: *I* is the *x*-coordinate of *P*, (positive in the strike-direction) and *J* defines the position of *P*, relative to *O*, in the up-dip direction (Figure 9). A least-squares estimate of the unknowns can be determined if observations of arrival time difference are available at four or more receivers.

The time intervals between the initiation pulse (subevent 1) and the two larger subevent arrivals (subevents 2 and 3) at the teleseismic stations shown in Figure 7 were combined with corresponding time intervals for the S-wave pulses at North Anna, and subevent P-wave arrival time intervals at the remaining local network stations shown in Figure 1. In the case of the teleseismic arrivals, the time measurement was aided by comparison of the recorded broadband velocity and acceleration waveforms with the synthetics developed as described above.

Figure 10 shows the results of the least-squares estimation of the locations of subevents 2 and 3, relative to subevent 1. To assess the resolution of the data, 500 locations for each subevent pair were performed, in each case randomly sampling only 1/2 of the available arrival time interval data set. The best estimates for the location and origin time of subevent 2, relative to subevent 1, using the full dataset, is X = 0.98 ± 0.12 km, Y = 0.85 ± 0.17 km with origin time difference 0.75 ± 0.01 s. For subevent 3, X = 1.48 ± 0.27, Y = 1.33 ± 0.39 km, and the time difference is 1.57 ± 0.03 s. The multiple relocations of the events using the random sampling indicate that the subevents are spatially resolved at different locations.

Note that the relative subevent location process used here is independent of the focal depth. The discrimination of the subevents from the surface reflections and the estimation of the focal depth was done by comparing synthetic seismograms (via Equation 12) with the actual recordings. Examples are shown in Figures 11 and 12, for velocity and acceleration waveforms, respectively. The best-fitting focal depth, which refers to the depth of rupture initiation (subevent 1), is 8.0 km. Most of the moment release was due to subevent 2, at a depth of 7.3 km: subevent 3 was at a depth of 7.0 km. Figure 13 compares the transverse velocity component simulation based on the absolute locations of the subevents and the synthetic waveform modeling with the actual recording at North Anna. The subevent source parameters used to generate the synthetics in Figures 11 through 13 are listed in Table 1.

**Absolute Location**

The aftershocks in the August 26 - September 2, 2011 period where used get an accurate epicenter location of the mainshock initiation. A select group of the best-recorded aftershocks were located with HYPOELLIPSE, using the velocity model derived here and all available *P* and *S*-wave arrival times from the stations shown in Figure 2. Three of the largest aftershocks in this group were well-recorded by several of the permanent stations shown in Figure 1. Those permanent stations also recorded the *P*-wave arrivals of the mainshock on-scale. An approach similar to that described above to locate the mainshock subevents 2 and 3 with respect to the initial subevent was used to determine the epicenter of the mainshock initiation with respect to each of the three aftershocks. The results were averaged, and the best-estimate of the epicenter of the mainshock initiation is 37.905°N, 77.975°W. The epicenter is shown as the red star in Figure 14. Subevents 2 and 3 are shown as red crosses in Figure 14. The uncertainty in the epicenter location is likely to be no more than 0.5 km, judging from the scatter of the three individual estimates. The surface projection of the rupture zone is centered approximately 1 km south of the intersection of State Route 605 (Shannon Hill Road) and State Route 646 (Yanceyville Road), in Louisa County, Virginia. The focal depth estimate of the rupture initiation is 8.0 km, with an uncertainty of approximately ± 1 km, based on comparison of observed teleseismic waveforms with synthetics.

## Discussion and Conclusions

The August 23, 2011 Virginia earthquake was a complex rupture featuring a small initial slip episode with moment roughly $2.5 \times 10^{16}$ N·m, followed 0.75 seconds later by a large subevent with a moment approximately $2.3 \times 10^{17}$ N·m which amounted to approximately 60% of the total moment release. A third subevent with moment $1.2 \times 10^{17}$ N·m occurred 1.57 seconds after rupture initiation. The three subevents appear to have involved a compact fault area, insofar as my best-estimate distance between subevents 1 and 3 is only 2.0 km. Given that the origin time difference between subevents 1 and 3 is a substantial 1.57 seconds, this implies a rupture velocity of only 1.3 km/s. The spatial and temporal location of subevent 2 is better constrained than that of subevent 3. The spatial separation of subevents 1 and 2 is 1.3 km, the time separation is 0.75 seconds, implying a rupture velocity of 1.7 km/s. However, nothing much was happening during most of the time between the onset of subevent 1 and subevent 2: subevent 1 was of short duration and very small moment release in comparison to subevent 2. My interpretation here is that the Virginia earthquake exhibited a very long total rise time, in comparison to the rupture area. This was a consequence of being comprised primarily of two short-duration energetic slip-events that were well-separated in time, along with a small, possibly low stress-drop, initiation event. An important issue is the effect this has on high-frequency ground motion amplitudes. Due to the complex nature of the source (multiple, energetic slip events with temporal gaps between slip episodes), the ground motion spectrum is highly modulated: parts of the *S*-wave spectrum exhibit amplitude reinforcement, while amplitudes at other frequencies are reduced. This sort of rupture process will contribute to substantial uncertainty in strong ground motion prediction, if the Virginia shock is characteristic of moderate eastern U.S. earthquakes generally.

The aftershock hypocenters define a tabular zone oriented in almost perfect agreement with the mainshock focal mechanism nodal plane. I find that the mainshock rupture occurred at depths between 7.0 and 8.0 km, at the base of the early aftershock zone. My location of the mainshock rupture zone is slightly beneath the projection of the plane defined by the aftershock hypocenters. This suggests that the mainshock may have occurred on a separate, but parallel, fault. A future study of the long-term behavior of the aftershock sequence may shed light on this.

The 8.0 km depth of rupture initiation is the median depth determined for previous shocks in the central Virginia seismic zone. Like previous earthquakes, both the mainshock and the aftershocks appear to be confined to allochthonous crystalline rocks of Paleozoic age. The aftershock hypocenters and focal mechanism do not rule out slip on either a Paleozoic or Mesozoic fault. The strike direction is not parallel to major Paleozoic structural trends. A projection of the aftershock hypocenters up-dip to the ground surface along the implied fault plane does not correlate with any previously mapped faults.

## Data and Resources

The data used for this study are readily available from the IRIS Data Management Center, http://www.iris.edu/hq/ , and by contacting the author.


## Acknowledgements

I thank John Maccrimmon and Dominion Inc., for providing strong motion data and related information. I think the citizens of Louisa County, Virginia, who graciously allowed me to deploy aftershock monitoring instruments in their backyards, under very stressful conditions. The author thanks all of his colleagues who responded to the Virginia earthquake by deploying instruments, and making the data immediately available to the seismological community. In particular, I thank Dr. Robert Herrmann and acknowledge his work to determine focal mechanisms, locate aftershocks, and to make that information available to all via the internet. I thank my old friends Matt Sibol and Jeff Munsey for providing first aid, constant support, insight and assistance with data collection and interpretation.


## References


Aki, K. and P.G. Richards (2002). *Quantitative Seismology*, 2nd Edition, University Science Books, Sausalito, California, 700p.

Bollinger, G.A. (1973a). Seismicity and crustal uplift in the southeastern United States, *American Journal of Science*, Vol. 273-A, 396-048.

Bollinger, G.A. (1973b). Seismicity of the southeastern United States, *Bulletin of the Seismological Society of America*, 63, 1785-1808.

Bollinger, G.A. (1969). Seismicity of the central Appalachian states of Virginia, West Virginia, and Maryland - 1758 through 1968, *Bulletin of the Seismological Society of America*, 59, 2103-2111.

Bollinger, G.A., A.C. Johnston, P. Talwani, L.T. Long, K.M. Shedlock, M.S. Sibol and M.C. Chapman (1991). Seismicity of the southeastern United States; 1698 to 1986, in *Neotectonics of North America*, D.B. Slemmons, E.R. Engdahl, M.D. Zoback and D.D. Blackwell, editors, Geological Society of America, 291-308.

Bollinger, G.A., M.C. Chapman and T.P. Moore (1980). Central Virginia Regional Seismic Network: Crustal Structure in Central and Southwestern Virginia, *NUREG/CR-1217*, U.S. Nuclear Regulatory Commission, Washington, D.C., 187 p.

Bollinger, G.A. and M.G. Hopper (1971). Virginia's two largest earthquakes - December 22, 1875 and May 31, 1897, *Bulletin of the Seismological Society of America*, 61, 1033-1039.

Brune, J.N. (1970). Tectonic stress and the spectra of seismic shear waves from earthquakes, *J. Geophys. Res.* **75,** 4997-5009.

Chapman, M.C. and R.W. Godbee (2012). Modeling Geometrical Spreading and the Relative Amplitudes of Vertical and Horizontal High-Frequency Ground Motions in Eastern North America, accepted for publication, *Bulletin of the Seismological Society of America*, in press, 2012.

Coruh, C., G.A. Bollinger and J.K. Costain (1988). Seismogenic structures in the central Virginia seismic zone, *Geology*, 16, 748-751.

Herrin, E. and Seismological Society of America (1968). 1968 Seismological Tables for P Phases, Introduction by E. Herrin, *Bulletin of the Seismological Society of America*, 58, 1193-1241.

Herrmann, R.B. (2011). St. Louis University Earthquake Center website, URL *http://www.eas.slu.edu/eqc/eqc_mt/MECH.NA/20110823175105/index.html*, last accessed July 5, 2012.

Hwang, Y.K. and J. Ritsema (2011). Radial Qu structure in the lower mantle from teleseismic body-wave spectra, *Earth and Planetary Science Letters*, 303, 369-375.

Kim, W-Y and M.C. Chapman (2005). The 9 December 2003, Central Virginia, Earthquake Sequence: A Compound Earthquake in the Central Virginia Seismic Zone, *Bulletin of the Seismological Society of America*, 95, 2428-2445.

Lahr, J.C., (1999). HYPOELLIPSE: a computer program for determining local earthquake hypocentral parameters, magnitude, and first-motion pattern: *U.S. Geological Survey Open-File Report 99–23*, version 1.1, 119 p. and software, available at http://pubs.usgs.gov/of/1999/ofr-99-0023/, last accessed July 5, 2012.

Munsey, J. and G.A. Bollinger (1985). Focal mechanism analyses for Virginia earthquakes (1978-1984), *Bulletin of the Seismological Society of America*, 75, 1613-1636.

Pratt, T.L., Çoruh, C., Costain, J.K., and Glover, III, L., 1988, A geophysical study of the Earth's crust in central Virginia: Implications for Appalachian crustal structure, *Journal of Geophysical Research*, v. 93, p. 6649-6667.

Taber, S. (1913). Earthquakes in Buckingham county, Virginia, *Bulletin of the Seismological Society of America*, 3, p. 124, NP1, 125-133.

Department of Geosciences

Virginia Tech

4044 Derring Hall

Blacksburg, VA 24061

mcc@vt.edu

Table 1

Source Parameters Used for Synthetic Seismograms

| *Subevent* | $M_o$ *(N·m)* | $\Delta\sigma$ *(MPa)* |
|---|---|---|
| 1 | $0.25 \times 10^{17}$ | 5 |
| 2 | $2.25 \times 10^{17}$ | 30 |
| 3 | $1.22 \times 10^{17}$ | 30 |

## Figure Captions

Figure 1. Triangles show the nearest stations recording the August 23, 2011 mainshock. The star shows the epicenter.

Figure 2. Terrain map (higher elevations colored brown) of the Louisa County, Virginia, area showing major roads. Red circles show epicenters of larger aftershocks, occurring from August 26, 2011 to January 12, 2012. Different symbols indicate temporary stations with different IRIS network designations, data from which have been archived at the IRIS Data Management Center: Virginia Tech temporary deployment (network XY, black triangles), IRIS Ramp deployment (network YC, black squares), USGS national strong motion program (network NP, black stars), USGS netquakes (network NQ, white triangles), USGS (network SY, black hexagons). The

epicenter of the mainshock initiation and two largest subevents are shown by the blue star and the blue crosses (see text).

Figure 3. (Top) Perspective view of the early (to September 2, 2011) aftershock hypocenters looking N29°E, in the strike direction of the mainshock focal mechanism nodal plane. (Bottom) Perspective view looking normal to the focal mechanism nodal plane.

Figure 4. (a) *S*-*P* arrival time interval versus *P*-wave arrival time for 36 aftershocks used to estimate upper-crustal velocity. The data have been arranged sequentially for display. The line indicates the joint estimate of the slope of Equation 4, ($v_p/v_s$ - 1). (b) Residuals from a least-squares fit to Equation 5, for *P*-wave travel-time (squared) versus epicenter distance (squared).

Figure 5. (a) Acceleration and velocity recordings at the foundation base-mat, Unit 1, Dominion Inc. North Anna power station. (b) Transverse component velocity recording (solid line) and full wavefield synthetic for a finite-fault simulation with a smooth source time function (dashed line). In (b), the observed data have been time-shifted to align the largest *S*-wave pulse, at 1.7 seconds in (a), with the far-field *S* waveform of the synthetic. Note the large *S*-wave pulse observed at approximately 6.5 seconds in (b) that is absent in the synthetic, as well as the small initial pulse observed at approximately 5.5 seconds in (b). All three observed *S*-wave pulses have polarity consistent with the mainshock focal mechanism. The *P*-wave arrival in the synthetic is at approximately 3.7 seconds in (b).

Figure 6. Selected teleseismic *P*- wave signals. Numbers indicate subevent arrivals.

Figure 7. Teleseismic stations used for analysis.

Figure 8. Dashed lines show wavefronts of direct *P*, *pP* and *sP* phases, arrows indicate ray directions and incidence angles. A constant ray parameter was assumed for a receiver at infinity. The time interval at the receiver between the direct *P* wave arrival and that of *pP* and *sP* is proportional to the distances along the ground surface shown by the bold arrows (see text).

Figure 9. 3-dimensional Cartesian coordinate system with origin at source point *O*. The position of a second source at point *P* is given by vector $\boldsymbol{V_{op}}$. Assuming a receiver at infinity, unit vector $\boldsymbol{V_r}$ indicates the ray directions at both *O* and *P*. Points *O* and *P* are assumed to lie in a fault plane defined by strike *s* and dip *d*. The source receiver azimuth is *a*, and the ray take-off angle (with respect to the negative z direction) is *toa*.

Figure 10. The result of 500 relative subevent locations, using random sampling with replacement, involving only 1/2 of the arrival time data set per sample. The locations of subevent 2 are shown by the circles, and subevent 3 by the crosses, relative to the location of subevent 1 (at X=0, Y=0). The coordinate system is in the fault plane (strike N29°E, dip 51°), with the positive X-axis in the strike direction.

Figure 11. Red lines show observed velocity waveforms (normalized to peak amplitudes) for stations ESK, ALE and YKW3. The green lines show synthetics created for different focal depths.

Figure 12. Red lines show observed acceleration waveforms (normalized to peak amplitudes) for stations ESK, ALE and YKW3. The green lines show synthetics created for different focal depths.

Figure 13. Solid line shows the recorded transverse component velocity record at North Anna. The dashed line shows a simulation based on the results of the subevent location and the subevent source parameters given in Table 1.

Figure 14. Circles show the epicenters of selected early aftershocks (August 26 - September 2, 2011) located using the velocity model determined in this study and all available recording stations. Red circles indicate the aftershocks used to determine the epicenter of the mainshock initiation (subevent 1), shown as the red star. The red crosses show the epicenters of subevent 2 and subevent 3.

Figure 15. (a) Crosses show hypocenters of early aftershocks (August 26 - September 2, 2011) located using the velocity model determined in this study and all available recording stations, projected onto a vertical plane with normal direction trending N29°E. Squares show the hypocenters of the mainshock initiation (subevent 1) and subevents 2 and 3. (b) as in (a), but projected onto a plane trending N29°E.

Figure
Click here to download Figure: figure1new.pdf

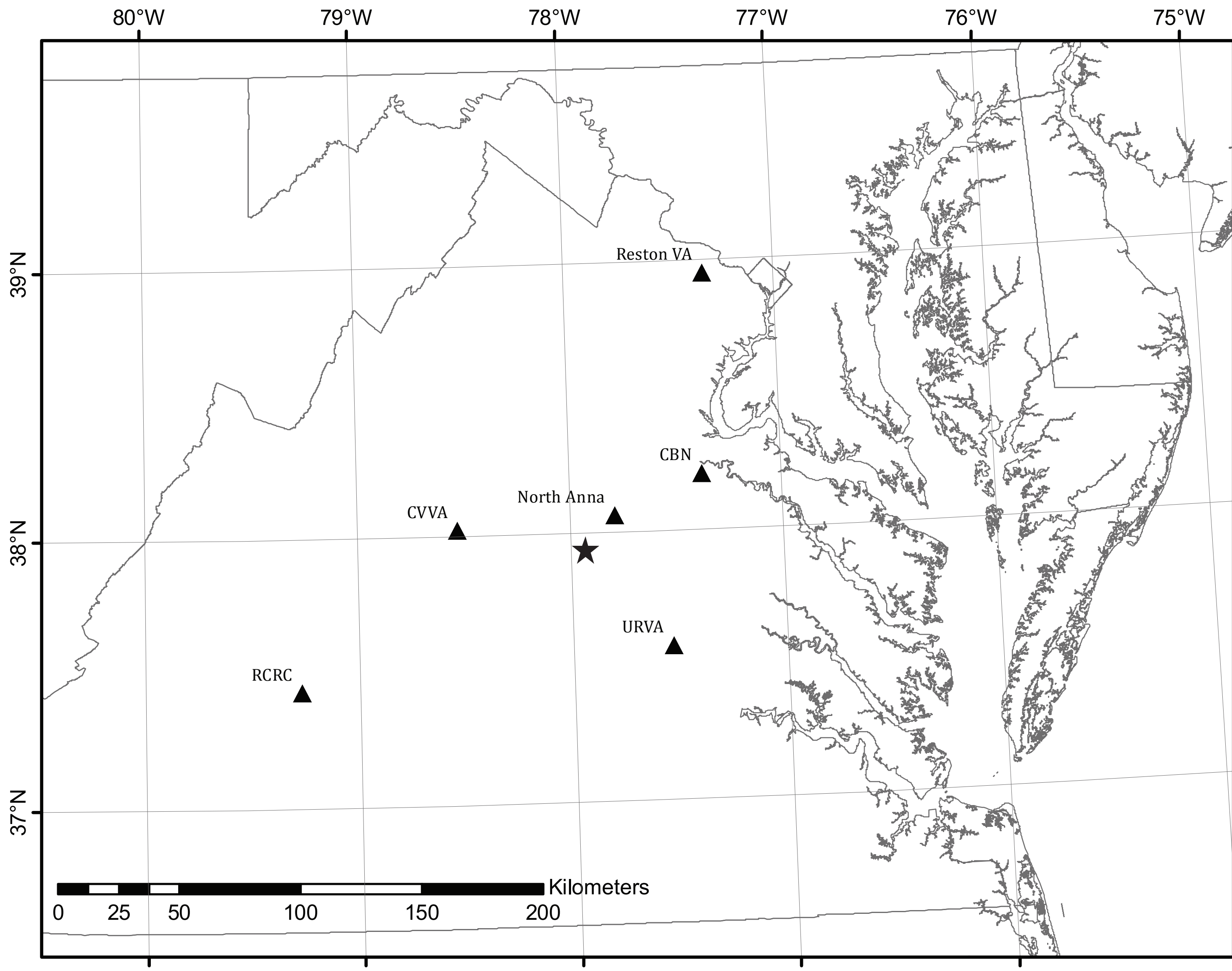

Figure
Click here to download Figure: figure2_new.pdf

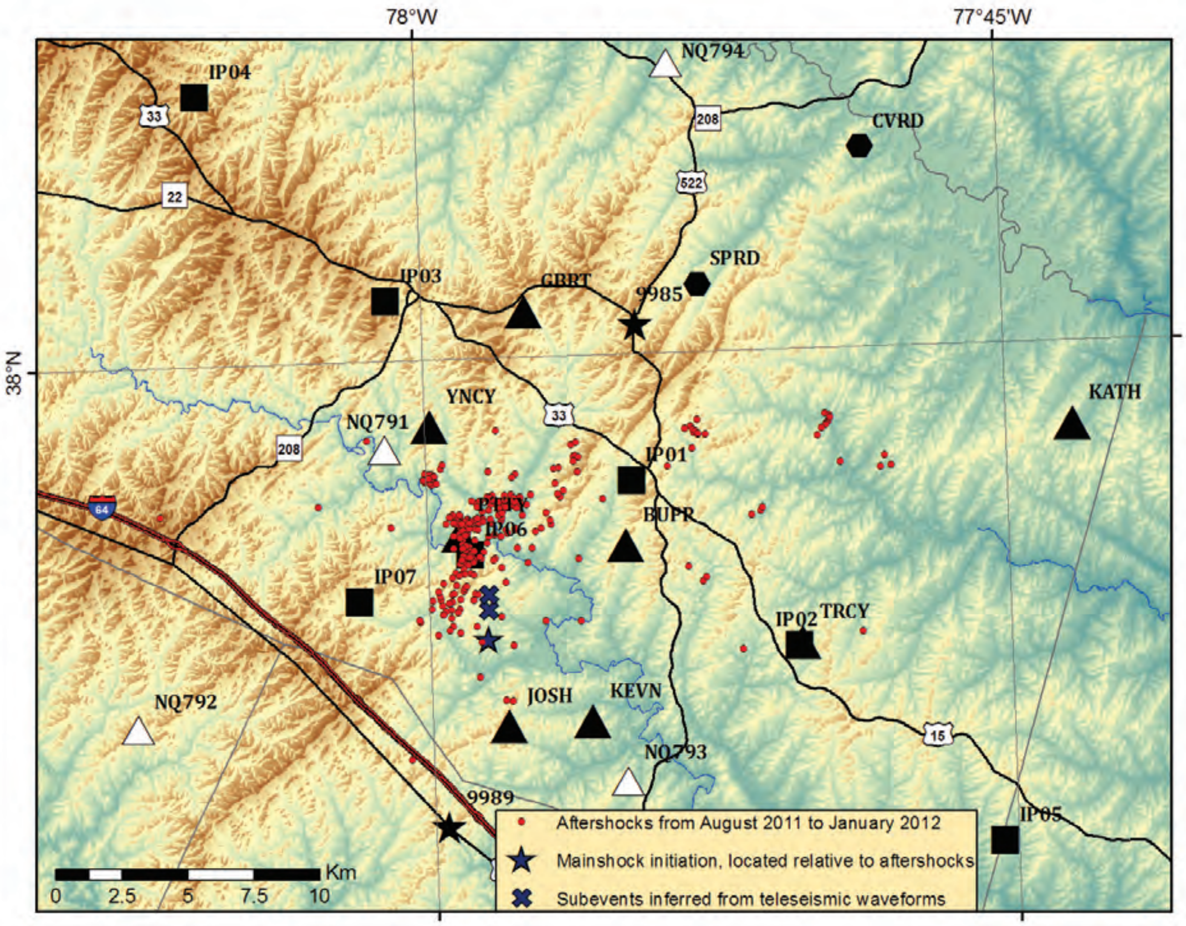

Figure
Click here to download Figure: figure3.pdf

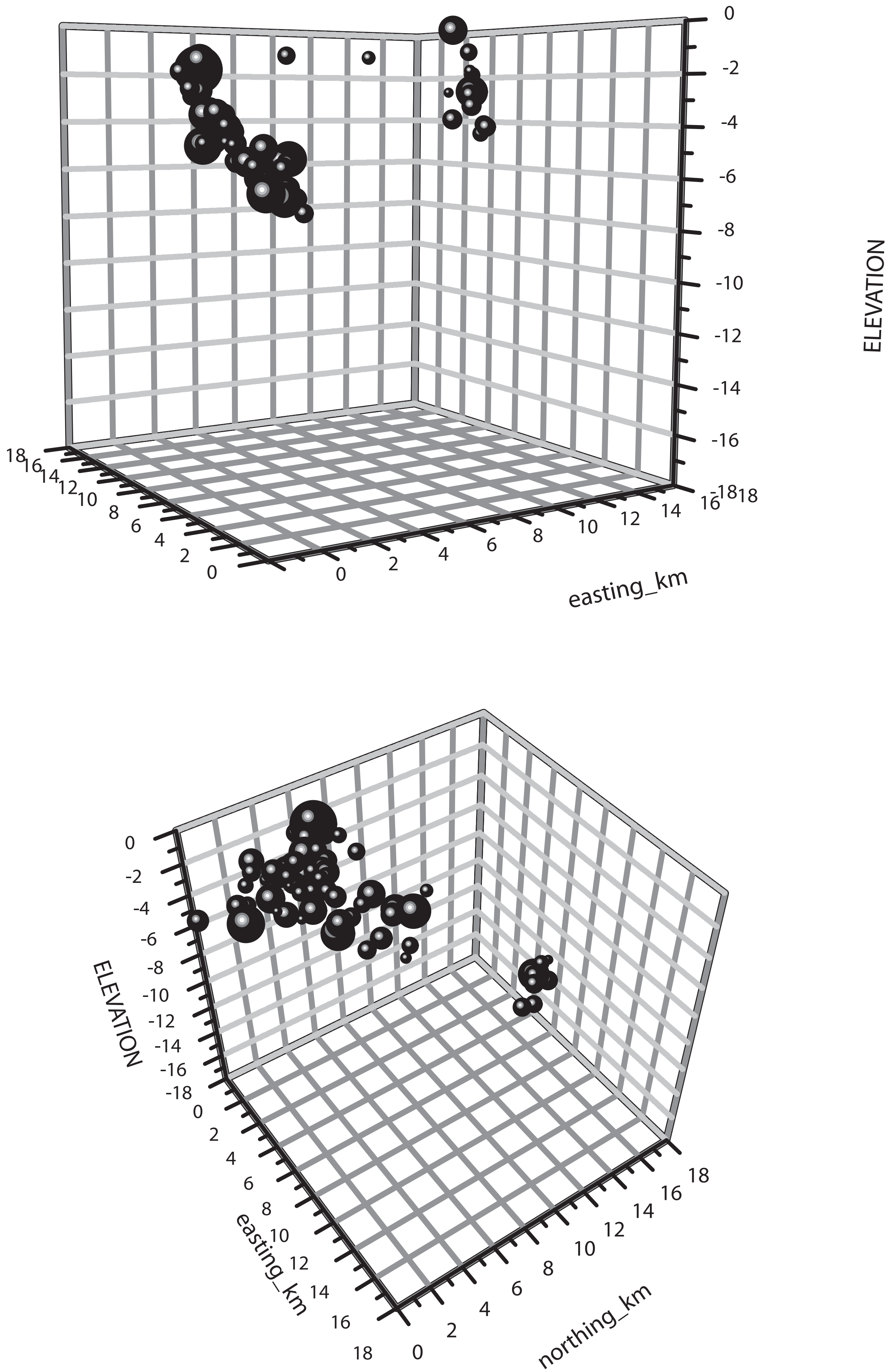

Figure
Click here to download Figure: figure4.pdf

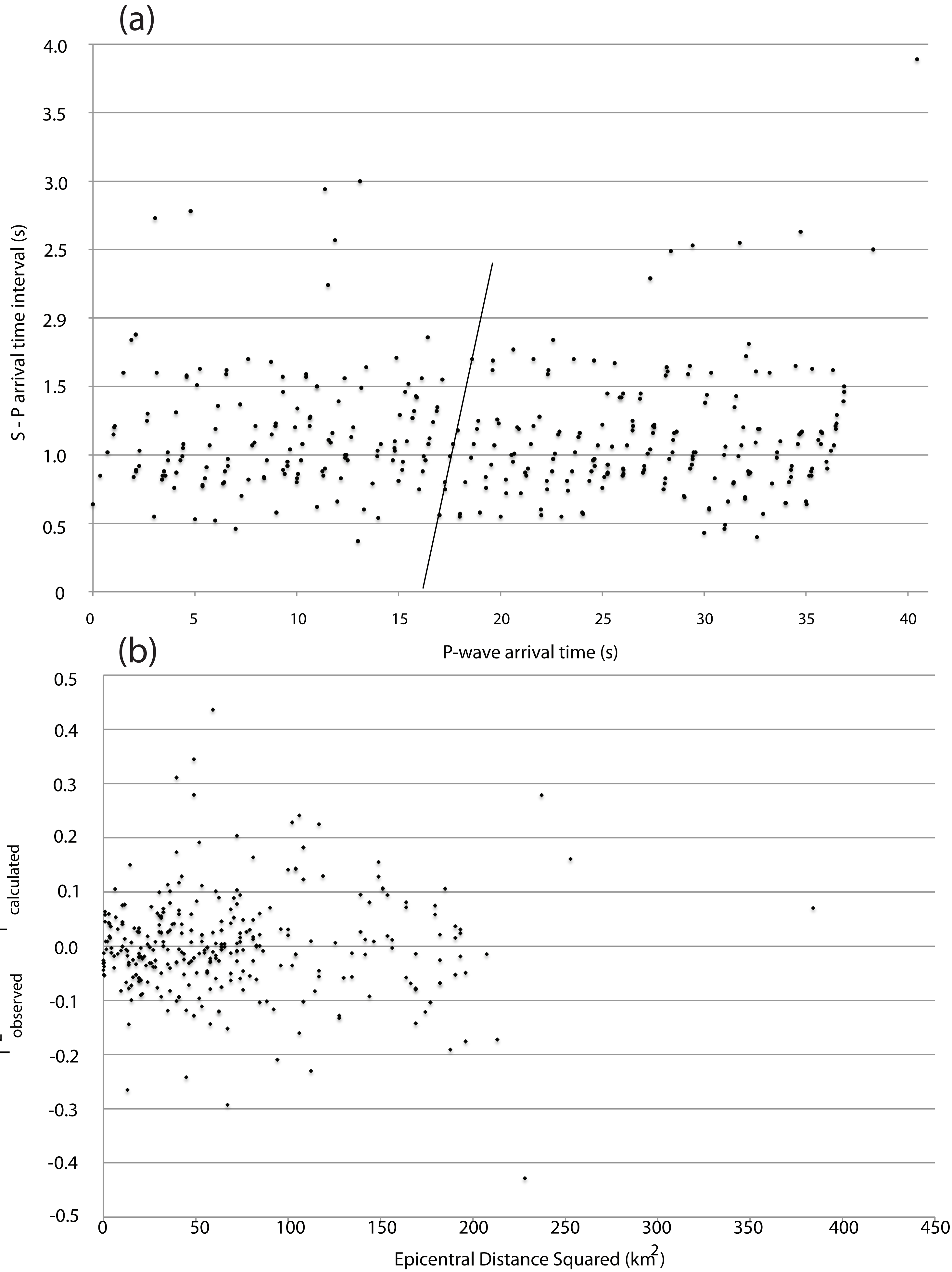

Figure
Click here to download Figure: figure5new.pdf

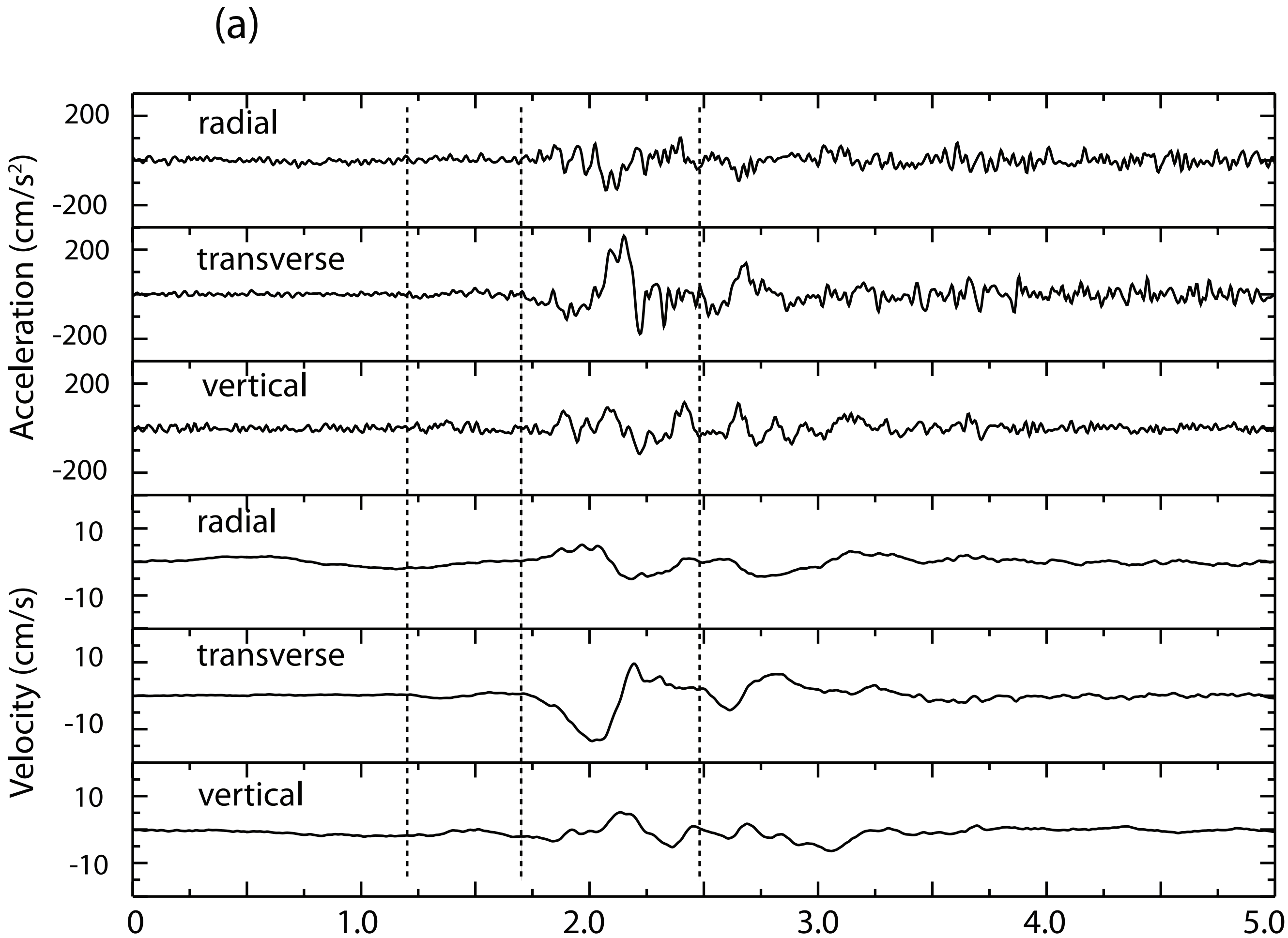


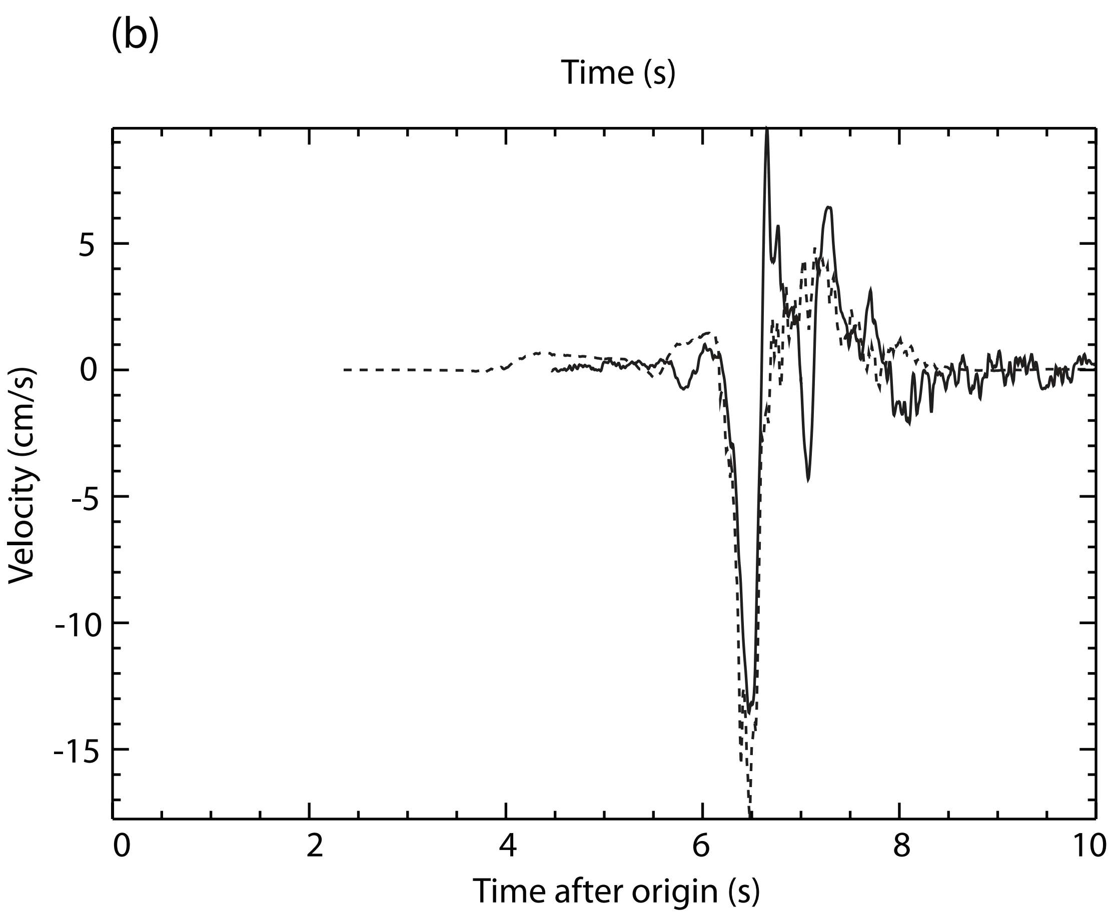

Figure
Click here to download Figure: figure6.pdf

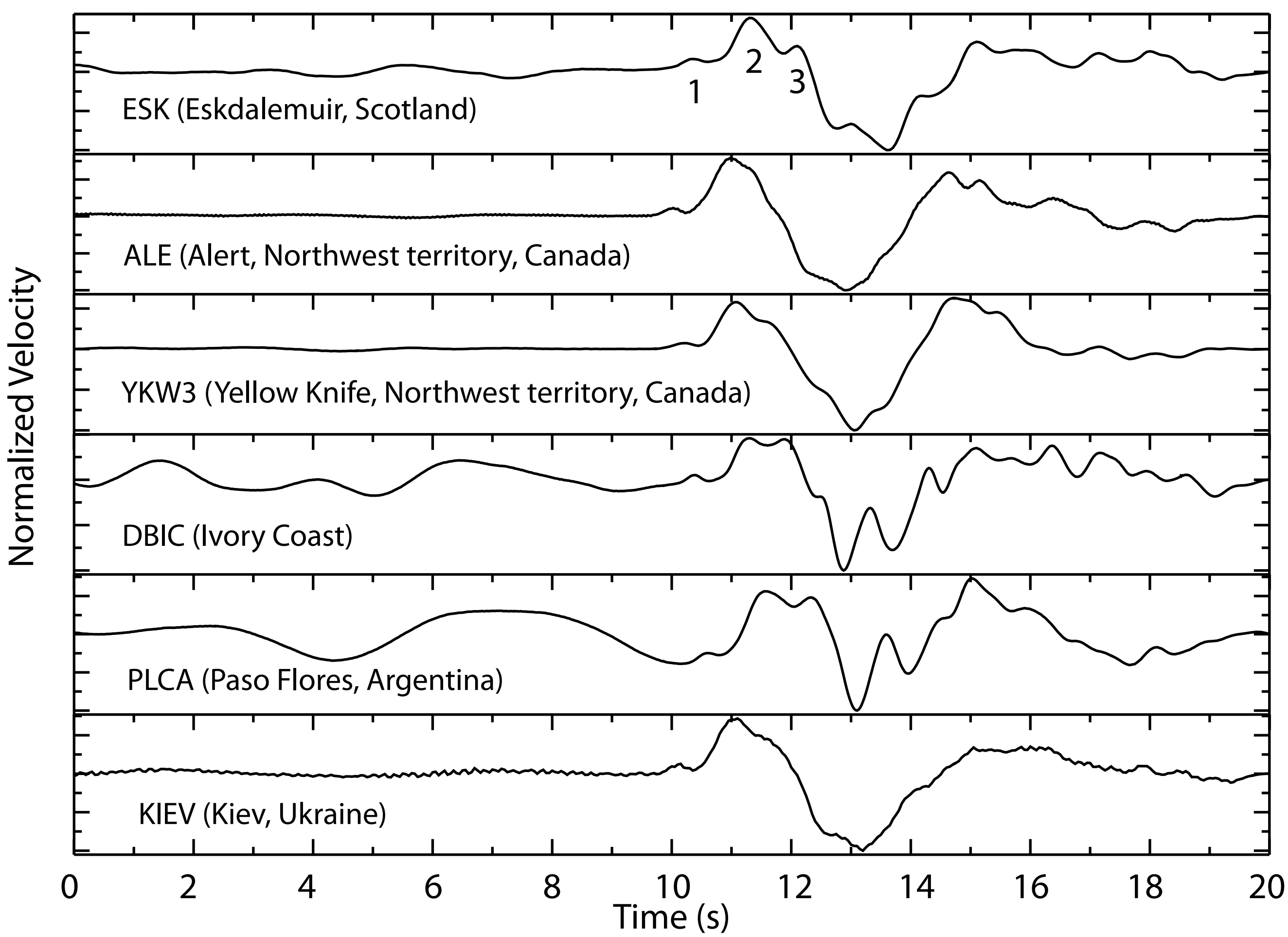

Figure

Click here to download Figure: figure7.pdf

Figure
Click here to download Figure: figure8new.pdf

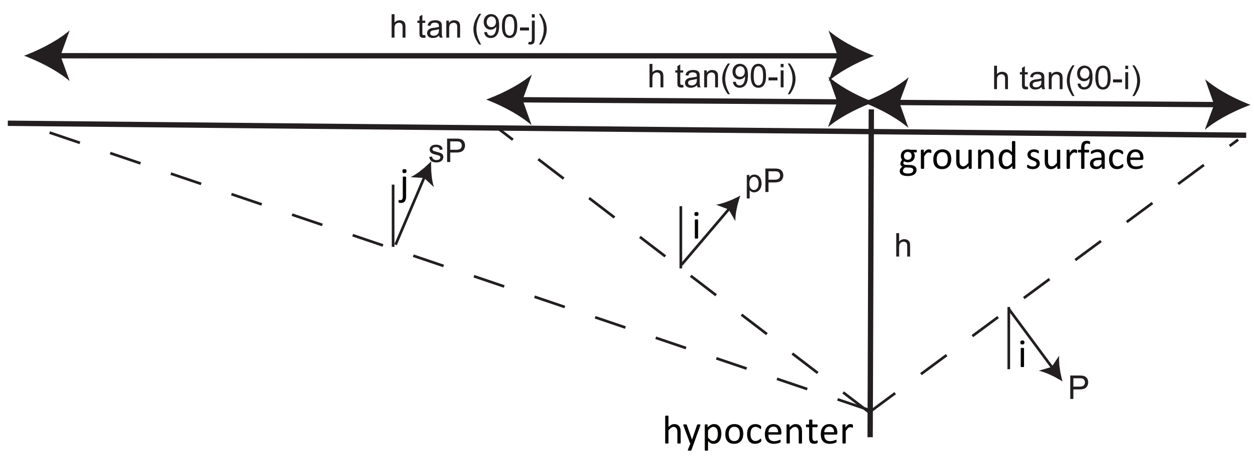

Figure

Click here to download Figure: figure9new.pdf

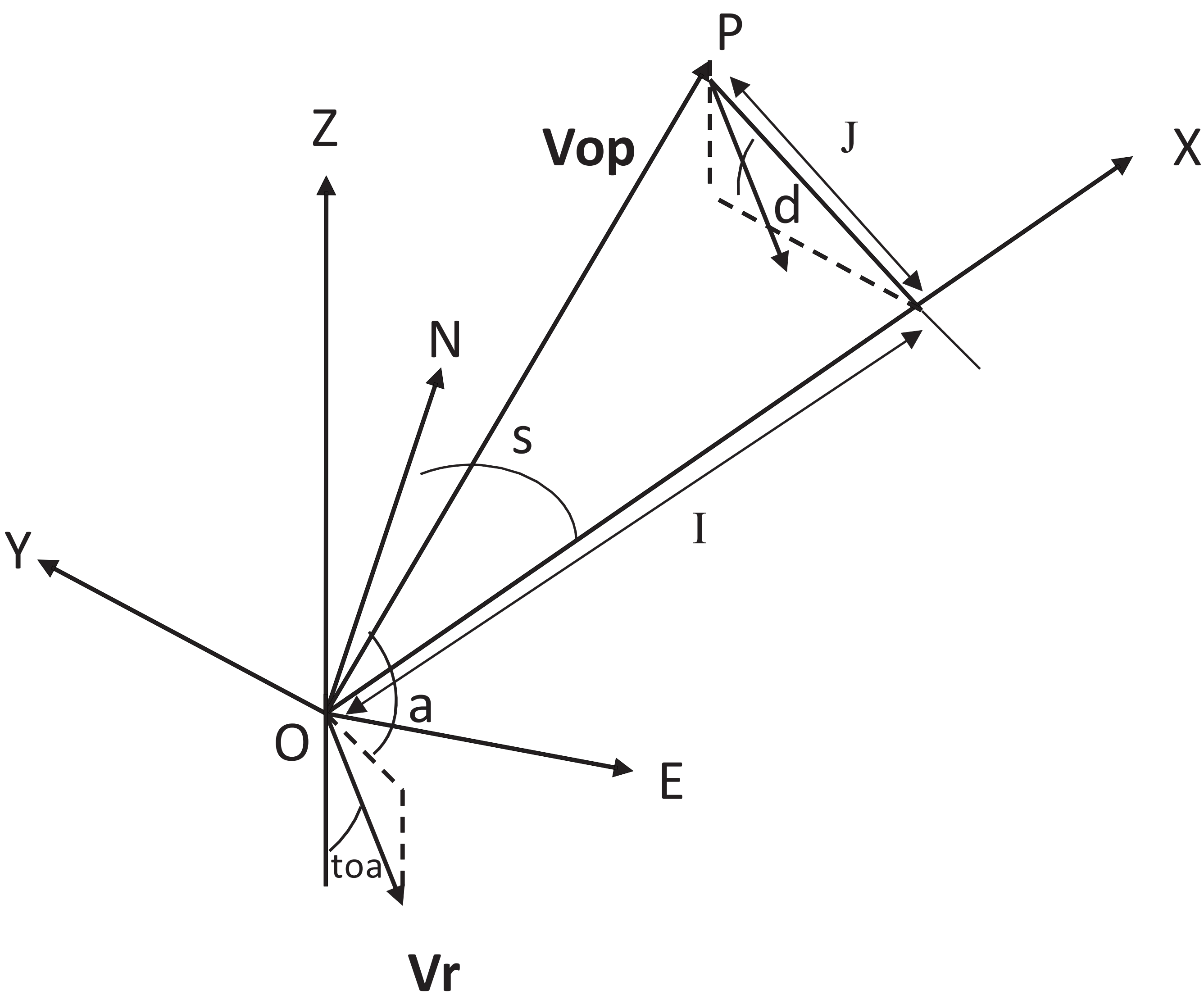

Figure
Click here to download Figure: figure10.pdf

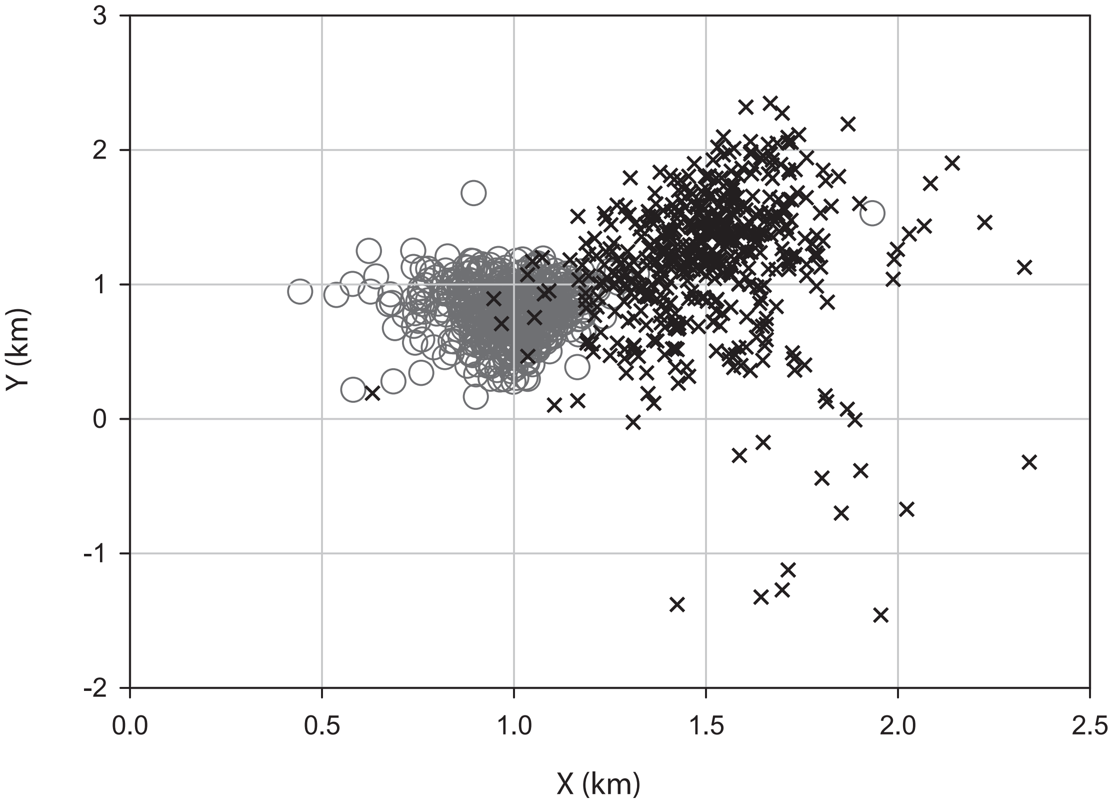

Figure
Click here to download Figure: figure11new.pdf

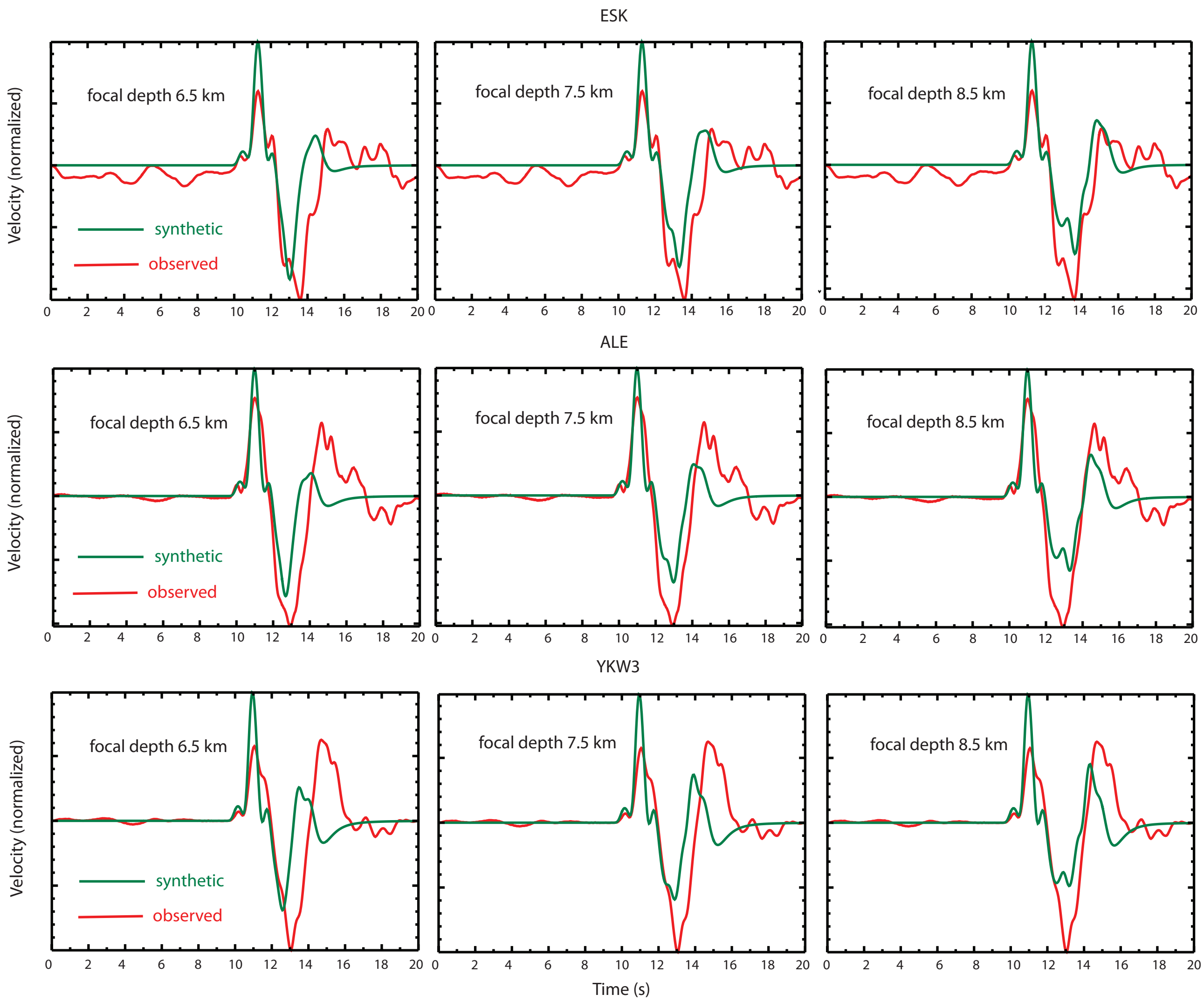

Figure
Click here to download Figure: figure12new.pdf

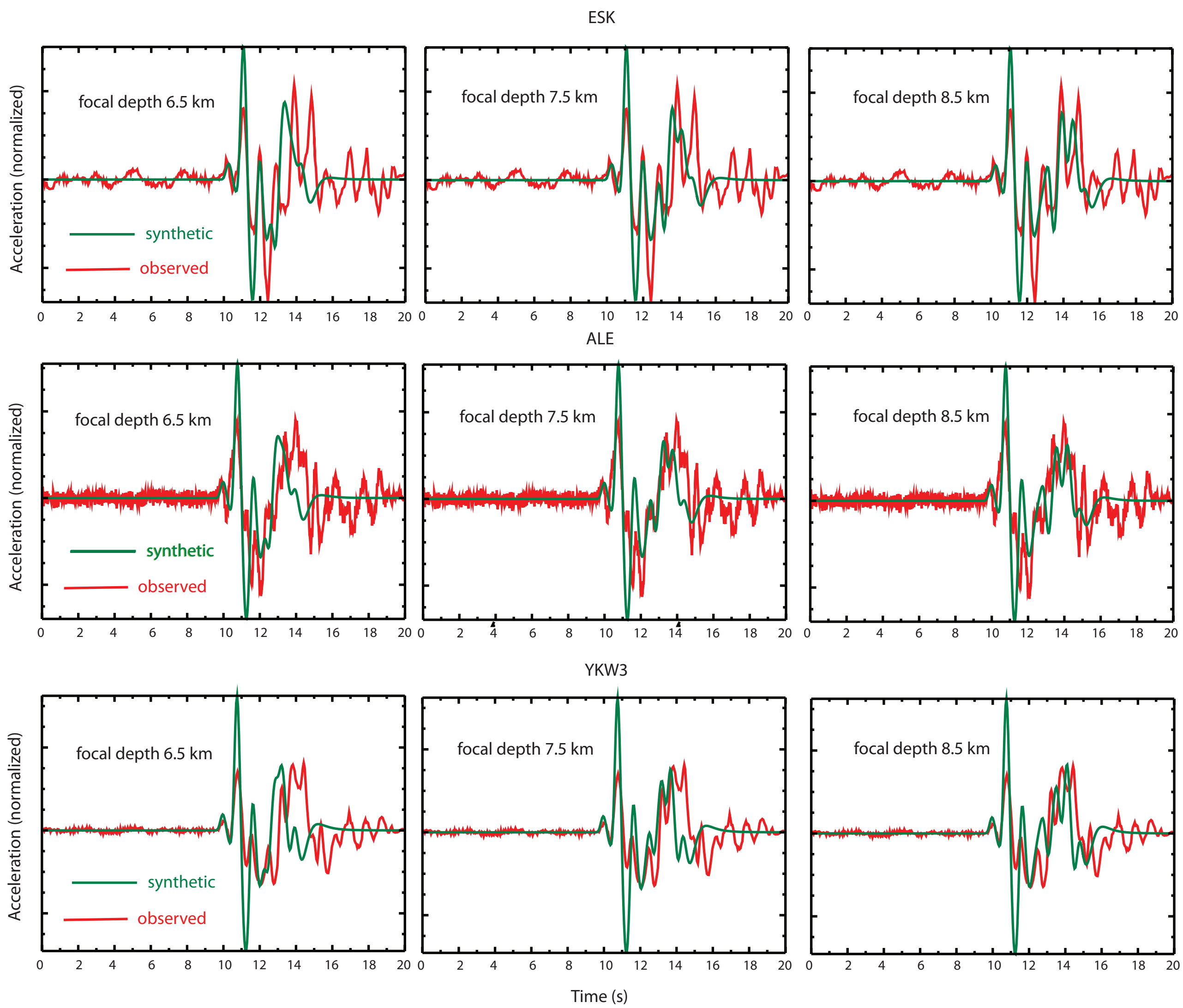

Figure
Click here to download Figure: figure13new.pdf

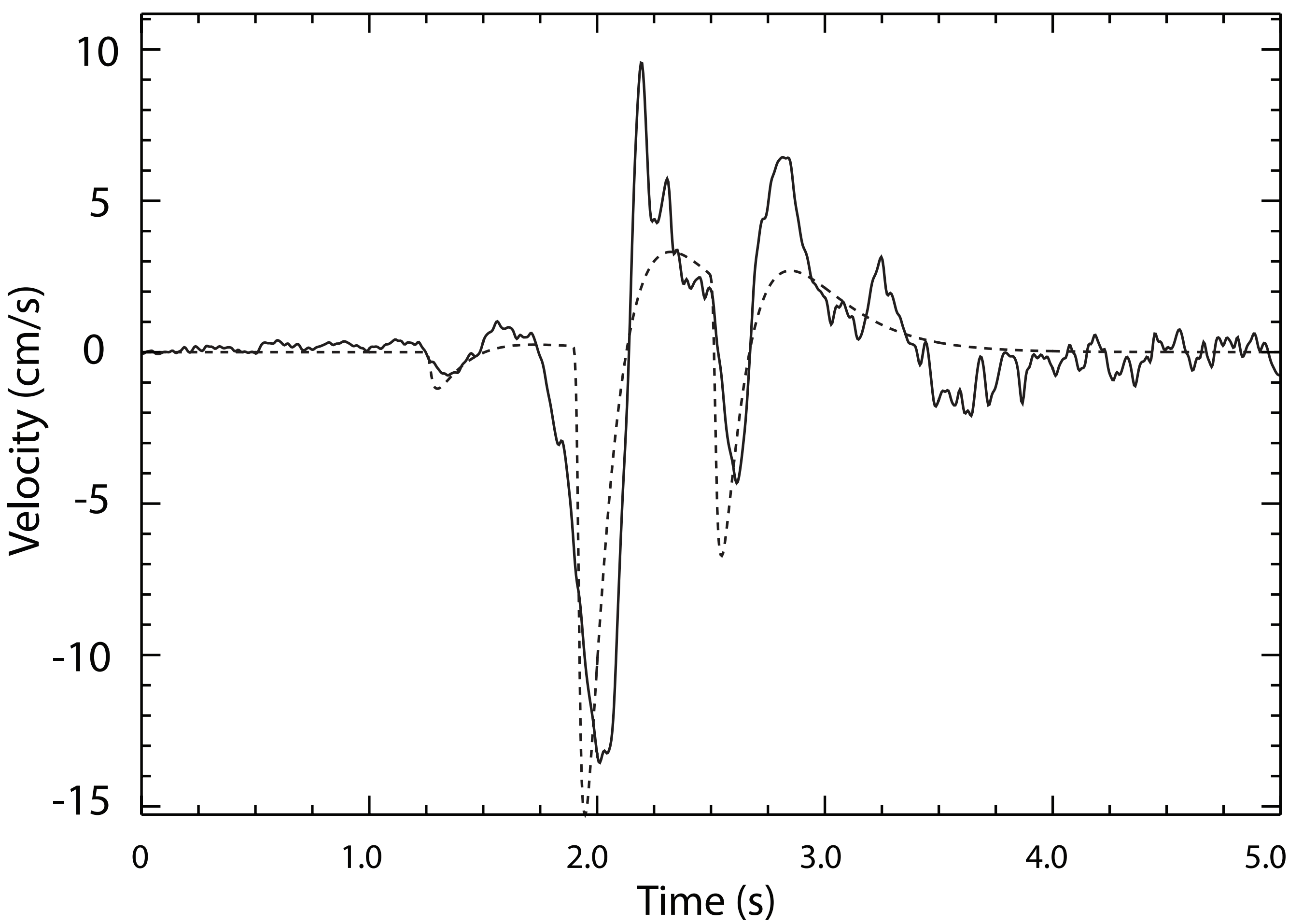

Figure

Click here to download Figure: figure14_new.pdf

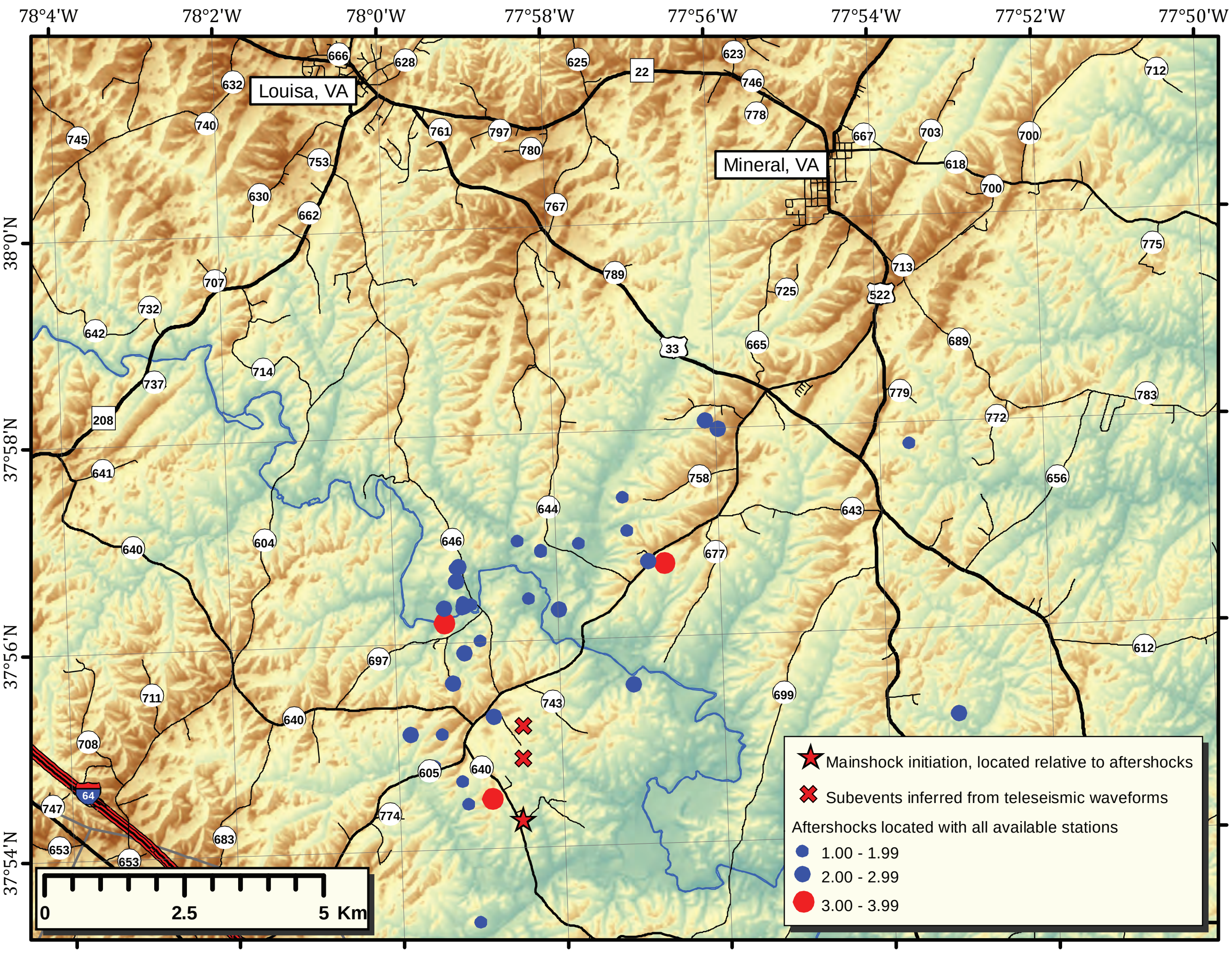

Figure
Click here to download Figure: figure15new.pdf

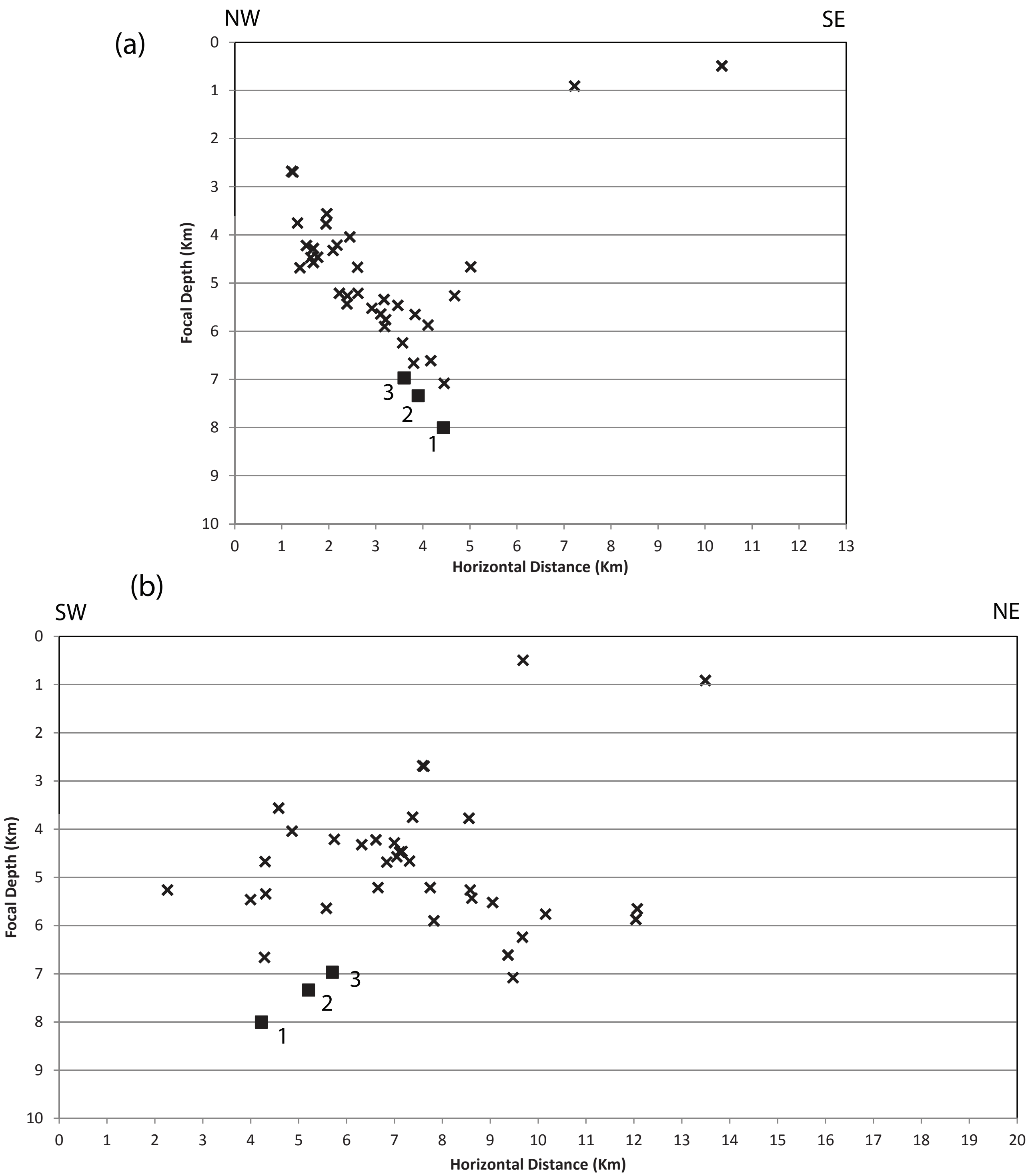

*Copyright Form
Click here to download Copyright Form: copyright.pdf

# *Bulletin of the Seismological Society of America*

## COPYRIGHT/PAGE-CHARGES FORM

**PLEASE FILL OUT AND SUBMIT THIS FORM ONLINE WHEN SUBMITTING YOUR PAPER OR FAX IT TO FAX NUMBER 503 405 7190**

Manuscript Number: BSSA-D-____________ [leave blank for new submissions]

Title: On the Rupture process of the August 23, 2011 Virginia Earthquake

Authors: Martin Chapman

### COPYRIGHT

In accordance with Public Law 94-533, copyright to the article listed above is hereby transferred to the Seismological Society of America (for U.S. Government employees, to the extent transferable) effective if and when the article is accepted for publication in the *Bulletin of the Seismological Society of America.* The authors reserve the right to use all or part of the article in future works of their own. In addition, the authors affirm that the article has not been copyrighted and that it is not being submitted for publication elsewhere.

To be signed by at least one of the authors (who agrees to inform the others, if any) or, in the case of "work made for hire," by the employer.

| Authorized Signature for Copyright | Print Name (and title, if not author) | Date |
|---|---|---|
| | MARTIN CHAPMAN | July 5, 2012 |

### PUBLICATION CHARGES

The Seismological Society of America requests that institutions supporting research share in the cost of publicizing the results of that research. The Editor has the discretion of waiving page charges for authors who do not have institutional support. Current rates are available at http://www.seismosoc.org/publications/bssa/authors/bssa-page-charges.php

**Color options**: Color figures can be published in (1) color both in the online journal and in the printed journal, or (2) color online and gray scale in print. Online color is free; authors will be charged for color in print. You must choose one option for all of the color figures within a paper; that is, you cannot choose option (1) for one color figure and option (2) for another color figure. You cannot submit two versions of the same figure, one for color and one for gray scale. You are responsible for ensuring that color figures are understandable when converted to gray scale, and that text references and captions are appropriate for both online and print versions. **Color figures must be submitted before the paper is accepted for publication. If color figures are changed to gray scale after acceptance of the paper, there will be a delay to publication while the paper undergoes further review by the Editorial Board.** Art guidelines are at http://www.seismosoc.org/publications/bssa/authors/bssa-art-submissions.php

Will page charges be paid? Check one:

__✓__ **BOTH PAGE CHARGES AND COLOR CHARGES WILL BE PAID**, and all color figures for this paper will be color both online and in print. This option requires full payment of page and color charges. ***Before choosing this option, please ensure that there is funding to support color in print.*** **See http://www.seismosoc.org/publications/bssa/authors/bssa-page-charges.php for current rates.**

_____ **ONLY PAGE CHARGES WILL BE PAID**, and all figures for this paper will be gray scale in print. Color figures, if any, will be color online.

_____ **A WAIVER OF PAGE CHARGES IS REQUESTED,** and all figures will be gray scale in print. Color figures, if any, will be color online.

Send Invoice To: Martin Chapman, Dept. Geosciences, Virginia Tech
4044 Derring Hall, Blacksburg, VA 24061

If your paper is accepted for publication, SSA requires that you fill out and submit an online billing/offprint form.

Questions regarding billing should be directed to SSA Business Office,
400 Evelyn Ave., Suite 201, Albany, CA 94706-1375 USA Phone 510 525-5474 Fax 510 525-7204